ORIGINAL PAPER

A new ~ 900-year varved record in Lake Walker, Québec North Shore, eastern Canada: insight on late Holocene climate mode of variability

Obinna P. Nzekwe · Francois Lapointe · Pierre Francus ·
Guillaume St-Onge · Patrick Lajeunesse · David Fortin · Jean-Philippe Jenny ·
Arnaud De Coninck · Édouard G. H. Philippe · Thibault Labarre

Abstract This paper presents a new annually laminated record (varves) from Lake Walker, Québec North Shore (eastern Canada) spanning the period from ∼ 3230 to 2320 ± 20 cal BP. A ∼ 3.5-m-long composite sequence was established with the best regular and continuous laminated intervals using computed tomography and high-resolution photographs. The varve chronology was built based on two methods: manual multi-parameter counting using the PeakCounter software, and manual counting on thin-section images obtained by scanning electron microscopy (SEM). The latter correlates more closely with the ages derived from AMS radiocarbon dating, suggesting that thin-section analysis is here a more reliable counting technique. Varves are clastic, composed of a silt layer deposited in spring and summer, and a clay layer deposited in winter. Annually resolved grain size obtained using image analysis technique on SEM images of thin sections and elemental composition from X-ray microfluorescence analyses performed on the floating varve chronology suggests that the record is sensitive to the North Atlantic Oscillation (NAO), as revealed by the strong co-variability with another lower resolution record from Greenland. This suggests that periods of negative winter NAO promoted a thicker snow cover that

Obinna P. Nzekwe and Francois Lapointe have contributed equally to this work.

Supplementary Information The online version contains supplementary material available at https://doi.org/10.1007/s10933-021-00220-x.

O. P. Nzekwe (✉) · F. Lapointe · P. Francus ·
D. Fortin · J.-P. Jenny · A. De Coninck · T. Labarre
Canada Research Chair in Environmental Sedimentology,
Centre - Eau Terre Environnement, Institut National de la
Recherche Scientifique, Québec, QC G1K 9A9, Canada
e-mail: obinna_peter.nzekwe@ete.inrs.ca

F. Lapointe
Department of Geosciences, Climate System Research
Center, University of Massachusetts, Amherst,
MA 01003, USA

P. Francus
GEOTOP Research Centre in the Dynamics of the Earth
System, Montréal, QC H2X 3Y7, Canada

G. St-Onge · É. G. H. Philippe
Canada Research Chair in Marine Geology, Institut des
Sciences de la mer de Rimouski (ISMER), Université du
Québec à Rimouski, Rimouski, Canada

P. Lajeunesse · T. Labarre
Département de Géographie, Université Laval, Québec,
QC G1V 0A6, Canada

D. Fortin
Department of Geography and Planning, University of
Saskatchewan, Saskatoon, SK S7N5C8, Canada

J.-P. Jenny
Université Savoie Mont Blanc, INRA, CARRTEL,
74200 Thonon-les-Bains, France

resulted in higher river discharges and stronger clastic component in the varves. In modern times, cooling of the North Atlantic in the mid 1970s to the late 1980s was also characterized by concurrent negative phase of NAO, which condition translated into increase snow precipitation over the region. Overall, these results highlight that the new Lake Walker varve record presents remarkable prospects of developing a longer and high-resolution paleoclimatological reconstruction of the NAO in a region where similar records are scarce.

Introduction

Annually laminated (varved) sediments can serve as reliable archives of past environmental conditions because of the quality of their chronology (Francus et al. 2013a; Lapointe et al. 2017; Ojala et al. 2012, 2013). Indeed, counting sediment successions deposited over the course of one year or less allows establishing precise varved-based chronologies with annual and/or seasonal resolution (Francus et al. 2013b; Jenny et al. 2013; O'Sullivan 1983; Ojala et al. 2012; Schnurrenberger et al. 2003; Zolitschka et al. 2015).

Annually resolved records of past climate conditions in the Québec North Shore (eastern Canada) region during the late Holocene are seldom (Zolitschka et al. 2015). To date, only instrumental data and paleoclimatic reconstructions from tree rings and stable isotopes from tree stems covering the past 200 years to the last millennium are available in northern Québec (Arseneault et al. 2013; Naulier et al. 2014; Nicault et al. 2014), while a new 160-year-long varved record from Grand Lake, Labrador, about 600 km to the north-east of the present study, is arising (Gagnon-Poiré et al. 2021). Nevertheless, annually laminated sediments from that period have been generally difficult to find in the region, hence, the

discovery of new varved sequences from this boreal region reported by Nzekwe et al. (2018) increased the prospects to reconstruct past regional modes of climate variability.

On the Québec North Shore, in the southeastern Canadian Shield (eastern Canada), three adjacent deep fjord lakes (lakes Pentecôte, Walker and Pasteur) were studied in order to evaluate laminae preservation and potential for varve formation. Facies analysis of short sediment cores using digital images and thin-sections revealed that the lakes contain bioturbated, partially laminated and well-laminated sediments (Nzekwe et al. 2018). It has been demonstrated that of the three earlier-studied lakes, Lake Walker is characterized by morphological factors that better favour the preservation of sediment laminae, which include higher relative depth, mean depth, maximum depth, critical depth and topographic exposure (Nzekwe et al. 2018). Based on comparison of laminae couplet counts to the chronology derived from ^{210}Pb measurements from a short core (core WA14-06-R from Lake Walker), the uppermost (recent) sediments are most likely to be annually laminated (Nzekwe et al. 2018). More so, it was suggested that laminated sediments in Lake Walker are better preserved in deeper parts of the lake based on laminae visibility index (LVI), a semi-quantitative index that was established using image observation of thin sections from core WA14-06-R (Nzekwe et al. 2018). However, the demonstration that laminations present in the deeper part of Lake Walker sedimentary sequence are annual has yet to be exposed.

The specific objectives of the present study are to: (1) produce a long continuous composite sequence from the set of parallel long cores that was collected from Lake Walker in March 2015, (2) establish an age model based on radiocarbon dating and laminations counting, evaluate the best varve counting technique and verify the hypotheses that laminated intervals in the composite sequence are varved, (3) characterize the laminations properties in order to evaluate the potential to extract a high resolution record of past climate from Lake Walker sediments.

Study site

Lake Walker (50° 16.02′ N, 67° 9′ W) is a picturesque lake situated on the Québec North Shore, north west of the Gulf of St. Lawrence in eastern Canada (Fig. 1A,

É. G. H. Philippe
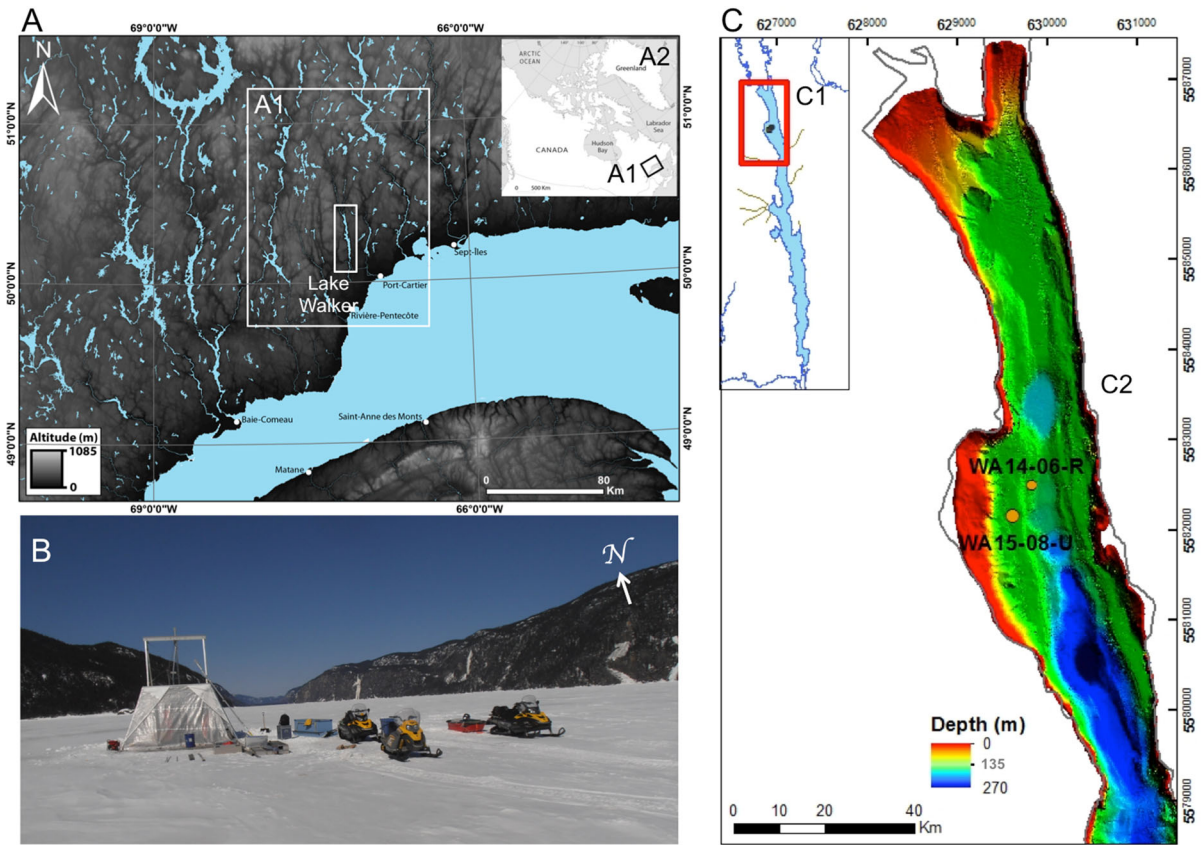Institut de Physique du Globe de Paris, Sorbonne Paris-Cité, UMR 7154 CNRS, Paris, France

Fig. 1 A Regional setting and geographic location of Lake Walker situated on the Québec North Shore (A1) in southeastern Canada, as shown in the insert (A2). **B** Panoramic view of Lake Walker (N-S direction) showing the materials used during fieldwork in March 2015. As shown, coring in Lake Walker posed technical challenges due to its remote location and geomorphology. **C** Map showing the northern part of Lake Walker (C1) that was cored. (C2) Multibeam bathymetry of the cored area (modified from Gagnon-Poiré et al. 2019). Also shown is the location of two cores: core WA14-06-R previously analysed (Nzekwe et al. 2018), and the composite core WA15-08-U (this study)

B). The maximum depth of the lake is 271 m (Gagnon-Poiré et al. 2019) (Fig. 1C) and the elevation above modern sea level is 115 m (Nzekwe et al. 2018). It has a ∼ 30-km-long predominantly longitudinal north-south oriented basin (Gagnon-Poiré et al. 2019). Morphologically, it is typically U-shaped, with steep sidewalls and relatively deep V-shaped bottom (150–271 m), and thus described as a fjord lake (Gagnon-Poiré et al. 2019; Lajeunesse 2014). It consists of two deep basins in the northern and southern parts, separated by a central sill. The area of the lake covers 41 km², while its watershed extends over 2187 km² (Gagnon-Poiré et al. 2019).

Lake Walker is dimictic and receives seasonal inputs of surficial material from two rivers, the Schmon and Gravel Rivers that flow into the northwestern and northeastern parts of the lake, respectively (Nzekwe et al. 2018). The headwaters of these rivers originate northwards from the boreal forests around Lake Manicouagan and the Caniapiscau River (Fig. 1A). The Québec North Shore has a subarctic climate where spring runoff occurs between April and May. Instrumental climatic data for the region are available from isolated meteorological stations, the closest being the Sept-Îles airport (50° 13′ 00″ N, 66° 15′ 00″ W, 52.60 m asl), which is ∼ 70 km east of Lake Walker (Centre d'expertise hydrique 2016). Detailed morphological and limnogeological characteristics of Lake Walker have been presented by Gagnon-Poiré et al. (2019), Normandeau et al. (2016) and Nzekwe et al. (2018).

Methods and materials

Sediment coring and construction of the composite sequence

The coring location was selected based on previously obtained multibeam bathymetric and subbottom profiler data (Gagnon-Poiré et al. 2019) and short sediment coring (Nzekwe et al. 2018) (Fig. 1C). A succession of core sections ranging from 100 to 200 cm in length were obtained from Lake Walker at a water depth of ∼ 140 m using a UWITEC piston corer on the lake ice cover (∼ 15 cm) in March 2015. The core sections were retrieved from two boreholes (08C and 08D), which were used to name individual core sections (Table 1, ESM 1). A gravity core was also retrieved at the site (08B-G). Collected sediment cores were stratigraphically realigned using marker beds (such as visible laminae, image artefacts and/or rapidly deposited layers) to construct a 352-cm-long composite sequence, WA15-08-U (Table 1, ESMs 2, 3). Hereafter, stratigraphical positions are expressed in centimeter composite depth (cm cd).

Computed tomography

Whole core sections were analysed using a SIEMENS SOMATOM Definition AS + 128 Volume Access sliding gantry medical CT-scanner (SIEMENS AG, Munich, Germany) at the *Institut National de la Recherche Scientifique, Centre Eau Terre Environnement* (INRS-ETE). The resulting images (0.6 mm resolution) were shown in gray scale. Gray scale values are expressed as CT numbers or Hounsfield units (HU), a proxy for sediment bulk density, porosity and mineralogy (Boespflug et al. 1995; Cremer et al. 2002; Fortin et al. 2013). Lighter and darker areas indicate higher and lower X-ray attenuations, respectively (St-Onge et al. 2007).

X-ray microfluorescence and X-radiography

An ITRAX core scanner with a molybdenum tube (Cox Analytical Systems, Mölndal, Sweden) was used to acquire microgeochemical (μ-XRF) and microdensity (radiography) variations in the split long sediment cores at INRS-ETE. Prior to measurement, RGB colour images (50 μm resolution) of the cores were taken using the ITRAX line scan camera. The number of counts for each element in a spectrum acquired for a specific depth interval was normalized by the total number of counts of that spectrum (expressed in counts per second, cps). "Inc" is the incoherent scattering or Compton scattering and "coh" is the coherent or Rayleigh scattering (Croudace et al. 2006). The inc/coh ratio is inversely proportional to the average atomic weight (Croudace et al. 2006). μ-XRF data was acquired at a down-core resolution of 100 μm at an exposure time of 5 s, using a voltage of 30 kV and current of 45 mA. Data were analysed using Q-Spec 8.6.0 software developed by Cox Analytical Systems (Croudace et al. 2006). Only elements that are well above the detection limit and that can be interpreted in a meaningful sedimentological way are discussed in this paper: they are Si, K, Ti, Fe, Ca and Zr. These μ-XRF data were annually

Table 1 List of sediment cores used to reconstruct the (∼ 4 m upper part of) composite core WA15-08-U (Lake Walker)

Core sections	Sections Length (cm)	Core sections depth interval (cm)	Core section depths used to construct composite (cm cd)
WA15-08B-G	143	0–143	0–139
WA15-08D-I-U-1	84	6–90	
WA15-08C-I-U-1	134	10–144	
WA15-08D-I-U-2	90	90–180	139–178*
WA15-08D-II-U-1	87.5	175–262.5	178–262.5*
WA15-08C-II-U-1	89	193–282	
WA15-08D-II-U-2	89.5	262.5–352	262.5–352
WA15-08C-II-U-2	96	282–378	

*Part of the composite core that was subsampled for thin-section analysis. Geographic location of core is shown in Fig. 1. Correlation panel of cores and list (including depths) of laminations that were used to reconstruct the composite sequence of are shown in ESM 2)

averaged in order to describe their variability in time (Lapointe et al. 2020). Additional high-resolution radiographs of the split cores were also obtained using a voltage of 50 kV, current of 45 mA and an exposure time of 700 ms.

Stratigraphy, chronology and radiocarbon dating

Terrestrial plant macrofossils (wood fragments) and bulk sediments (in the absence of datable fossils) were collected at various depths from the composite core WA15-08-U (Table 2). The samples were prepared for ^{14}C dating at the *Centre d'études Nordiques* (CEN), *Université Laval* and analysed using accelerator mass spectrometry (AMS) at the Earth System Science Department Keck Carbon Cycle AMS Facility at the University of California at Irvine. The dates were calibrated using Calib 7.1 software using the Northern Hemispheric calibration curve INTCAL2013 (Reimer et al. 2013). The age-depth model was established using the Clam software version 2.2 (Blaauw 2010a) interface with the R software (Blaauw 2010b), which allowed for plotting the "best fit" with 95% confidence interval. For the reconstruction of the varve chronology, only the ^{14}C ages within the selected sediment depth interval were considered (Table 2).

Lamination and varve counting

A semi-quantitative index, the "Lamination visibility index (LVI)" was used to describe the visibility of laminations: 0—none, 1—faint, 2—visible, 3—clear, and 4—distinct on the composite sequence WA15-08-U, using similar method as Nzekwe et al. (2018). Two varve counting methods were tested on the 175–263 cm cd interval of core WA15-08-U (Table 1) having the best LVI indices: manual counting using the PeakCounter software, and manual counting on thin-sections supported by image analysis.

Manual counting using PeakCounter

A multi-parameter approach of manual counting using the freeware PeakCounter 1.6.4 (Marshall et al. 2012) was used to count the laminations on core WA15-08-U (∼ 175–263 cm cd). In order to analyse the laminations, the X-ray radiograph (with gray scale values), optical image (from ITRAX line scan camera) and (XRF) elemental variations (Si, Ti, K, Fe and Ca) and

also the inc/coh ratio were evaluated adjacently. These elements were selected because they were the ones following better the varves components, yet allowing the best varve identification (Marshall et al. 2012; Nakagawa et al. 2012). The following pre-defined criteria were set in order to facilitate varve counting using PeakCounter: (1) the μ-XRF was run at a high resolution (100 μm) such that peaks in elemental compositions would represent sub-layers in the laminae couplet (varve) structure, and (2) the μ-XRF step size and the X-radiography resolution were the same (100 μm) in order to facilitate correlation of XRF elemental composition and digital images. Considering the mean laminae couplet thickness of ∼ 0.7 mm (minimum laminae couplet thickness is 0.18 mm, maximum laminae couplet thickness is 3.85 mm and the standard deviation is 0.57) in the uppermost (recent) sediments from Lake Walker (Nzekwe et al. 2018), seven μ-XRF measurements (0.1 mm) were obtained on average per laminae couplet.

Similar to the LVI, a varve quality Index (VQI) was used to describe how XRF elemental peaks within the PeakCounter 1.6.4 software correlate with laminae boundaries of the selected core section (∼ 175–263 cm cd): VQI 1: faint—where medium to low peaks in two or less XRF elements correlate but do not clearly correspond with laminae/varve boundaries in the digital images; VQI 2: visible—where medium to low peaks in at least three elements correlate and do not clearly correspond with laminae/varve boundaries in the digital images; VQI 3: clear—where high to medium peaks/lows in at least four XRF elements correlate and are distinguishable with laminae/varve boundaries in the digital images; VQI 4: distinct—where high peaks/lows in all selected XRF elements correlate and correspond with laminae/varve boundaries in the digital images. Hence, VQI 4 represents the best quality.

Thin-section counting, image analysis and particle size analyses

Undisturbed sediments were subsampled using aluminium slabs (measuring 8 × 1.5 × 0.5 cm), freeze-dried and epoxy-resin embedded based on the methods by Francus and Asikainen (2001) and Lamoureux (1994). The thin-section slabs were scanned at 2400 dpi in plain and cross-polarized light to obtain digital images using an Epson transparency flatbed unit. Then

Table 2 AMS ^{14}C age of dated materials from the composite core WA15-08-U (Lake Walker)

Core name	Material	Core section depth (cm)	Composite Depth (cm cd)	UC Irvine Lab #	Université Laval #	^{14}C a BP	^{14}C cal BP
WA15-08D-I-U-1	Bulk sediment	45	47	UCIAMS-179151	ULA-6395	980 ± 15	891 ± 40
WA15-08D-I-U-2	Bulk sediment	10.5	104.5	UCIAMS-179152	ULA-6396	1265 ± 15	1223 ± 30
WA15-08C-I-U-1	Wood fragment	119	128	UCIAMS-179988	ULA-6442	1565 ± 15	1466 + 40
WA15-08D-I-U-2	Bulk sediment	51	145	UCIAMS-179153	ULA-6397	1750 ± 15	1666 ± 30
WA15-08D-II-U-1	Bulk sediment	6	176	UCIAMS-179953	ULA-6399	2735 ± 15	2803 ± 20*
WA15-08D-I-U-2	Wood fragment	32	179	UCIAMS-179985	ULA-6441	2370 ± 15	2361 + 5
WA15-08D-I-U-2	Bulk sediment	89	207	UCIAMS-179154	ULA-6400	2320 ± 15	2347 ± 20
WA15-08D-II-U-1	Bulk sediment	41.5	217.5	UCIAMS-217742	ULA-8512	2765 ± 20	2853 ± 30
WA15-08D-II-U-1	Bulk sediment	65	241	UCIAMS-217743	ULA-8513	3035 ± 20	3272 ± 40
WA15-08D-II-U-1	Bulk sediment	85	260	UCIAMS-179954	ULA-6400	3190 ± 15	3417 ± 20*
WA15-08D-II-U-2	Bulk sediment	11	273	UCIAMS-179955	ULA-6401	3360 ± 15	3608 ± 20
WA15-08D-II-U-2	Bulk sediment	50	312	UCIAMS-179956	ULA-6402	3785 ± 15	4169 ± 50
WA15-08D-II-U-2	Bulk sediment	88	350	UCIAMS-179979	ULA-6435	6180 ± 15	7081 ± 15

Two of the outliers (at 176 and 207 cm cd) are located near the depth interval where there is an age reversal (between 176 and 179 cm cd). These samples were sampled near the (∼ 5 cm) edge of the individual core sections that make up the composite sequence (Table 1, ESMS 1, 2), where some disturbance, and possible contamination can occur

*Dates from the test interval of the composite core (cm cd) from which thin-section were subsampled. Correlation panel of core sections is shown in ESM 2

these digital images were used for lamination counting using an in-house software developed at INRS-ETE (Francus and Nobert 2007). Varve counting was done by two different researchers (O.P.N and F.L). An error estimate was calculated based on the difference in the number of laminae couplets in each thin-section divided by the total varves expressed in percentage (Zolitschka et al. 2015).

Regions of interest (ROIs) on the flatbed digital scans were identified using the in-house software (Francus and Nobert 2007) and images of these ROIs were automatically acquired using SmartSEM software and further analysed using a Zeiss Evo50® scanning electron microscope (SEM) in backscattered

electron (BSE) mode at INRS-ETE. 8-bit gray-scale BSE 1024 × 768 pixels images, with a pixel size of 1 μm, were obtained at a tilt angle of 0°, working distance of 8.5 mm, and accelerating voltage of 20 kV, in order to optimize contrast between clastic grains and clay matrix (Francus et al. 2008; Lapointe et al. 2012). Approximately 1000 BSE images were analysed such that clay matrix and clastic particle appeared in white and black, correspondingly. Within each laminae couplet (clay and clastic lamina) every individual particle size was measured by image analysis (Francus 1998), and the following particle size distribution (PSD) indices were calculated: medium disk apparent diameter (mD_0) (Francus

1998), standard deviation (sD_0), maximum disk apparent diameter ($maxD_0$), and percentiles of particle size distribution $P75D_0$, $P95D_0$, $P98D_0$ and $P99D_0$, using a similar method as Lapointe et al. (2019) and Gagnon-Poiré et al. (2021). Subsequently, the Lake Walker varved record was compared with other records that are highly resolved and well dated in the time interval corresponding to the 175–263 cm cd interval of core WA15-08-U.

Statistical analysis of proxy data

The physical properties of the laminated sediments such as varve thickness (VT) and particle-size indices (D_050, sD_0, $P75D_0$, $P95D_0$, $P98D_0$ and $P99D_0$, and $maxD_0$) were analysed using the Paleontological Statistic (PAST) software (Hammer et al. 2001). Univariate analysis was used to calculate measures of location (mean and median), and measures of spread (variance and standard deviation). Normality test using Shapiro–Wilk test indicated that the sample data (VT and particle-size indices) were not normally distributed (ESM 4), thus statistical correlation of VT and particle size variables was done using a non-parametric test, the Spearman's rank order correlation coefficient (r_s) (Dodge 2003; Hammer et al. 2001). Principal component analysis (PCA) was used to transform the multivariate XRF elements into groups that highlight similarities and differences (Hammer et al. 2001).

Results

Sediment description

The laminae couplets from the core WA15-08-U ($\sim$ 175–263 cm cd) comprise two main lithologic layers: a fine silt layer rich in Ti and Zr, and a clay-rich layer with small amount of barely visible diffuse and degraded organic matter rich in Fe (Fig. 2). No diatom or other recognizable organic component was visible regularly in one of the components of the varves. The clay-rich layer, otherwise referred to as clay cap (Francus et al. 2008; Zolitschka et al. 2015) was the main feature used to delineate the laminae couplet boundaries due to their relatively fine and more distinct borders compared to the silt-rich layer (Fig. 2B). Three depositional events with thicknesses

of $\geq$ 1 cm characterized by relatively high gray scale value, high Fe, medium Mn and high Si and Ti (not shown) were found at $\sim$ 240, 241 and 246 cm cd respectively (ESM 5). They are interpreted as rapidly deposited layers (St-Onge et al. 2007, 2012) and were used to correlate cores between them in the establishing of the composite profile.

Univariate analysis of varve thickness (VT) and particle size data (mD_0, sD_0, $P75D_0$, $P95D_0$, $P98D_0$ and $P99D_0$, and $maxD_0$) extracted from the test interval of core WA15-08-U (175–263 cm cd) is presented in Table 3. The mean VT is 0.86 mm (minimum VT is 0.17 mm, maximum VT is 7.62 mm) with variance of 0.29 mm and standard deviation of 0.54 mm (Table 3). Spearman's rank correlation indicates that there is a low, positive, monotonic association (n = 923, $p < 0.01$) between VT and particle size parameters (mD_0, sD_0, $P75D_0$, $P95D_0$, $P98D_0$ and $P99D_0$, and $maxD_0$) (Table 4). Although the correlation coefficient (Spearman's rank order coefficient, r_s) is generally low ($r_s < 0.2$) for all variables, the strongest correlation with varve thickness is obtained with the 75th percentile ($r_s = 0.2184$, p value = 0.0001; Table 4).

Stratigraphy, chronology and radiocarbon dating

The results of thirteen radiocarbon ages obtained from the laminated intervals in the composite core WA15-08-U (0–352 cm cd) from Lake Walker are presented in Table 2. The radiocarbon based age-depth model (Fig. 3A) is constrained by ten AMS ^{14}C dates that span from 4169 $\pm$ 50 cal BP to 891 $\pm$ 40 cal BP. This corresponds to the late Holocene sedimentation. Three dates derived from bulk sediment sampled at 176, 207 and 350 cm cd, respectively were considered as outliers because they were plotted outside the line of best fit (marked in red colour; Fig. 3A). Using the age model, the mean sedimentation rate in Lake Walker during the last $\sim$ 4 ka BP ranges from 0.52 to 1.75 mm a^{-1}, based on radiocarbon dating.

The sediment interval that was selected for varve studies ($\sim$ 175 to 263 cm cd) spans from 3417 $\pm$ 20 cal BP to 2347 $\pm$ 20 cal BP (Fig. 3B). Besides the outliers (as noted above), an age reversal was noticed on the upper part of the selected section, where bulk sediments sampled at 176 cm cd dated 2803 $\pm$ 20 cal BP, while wood fragment sampled at
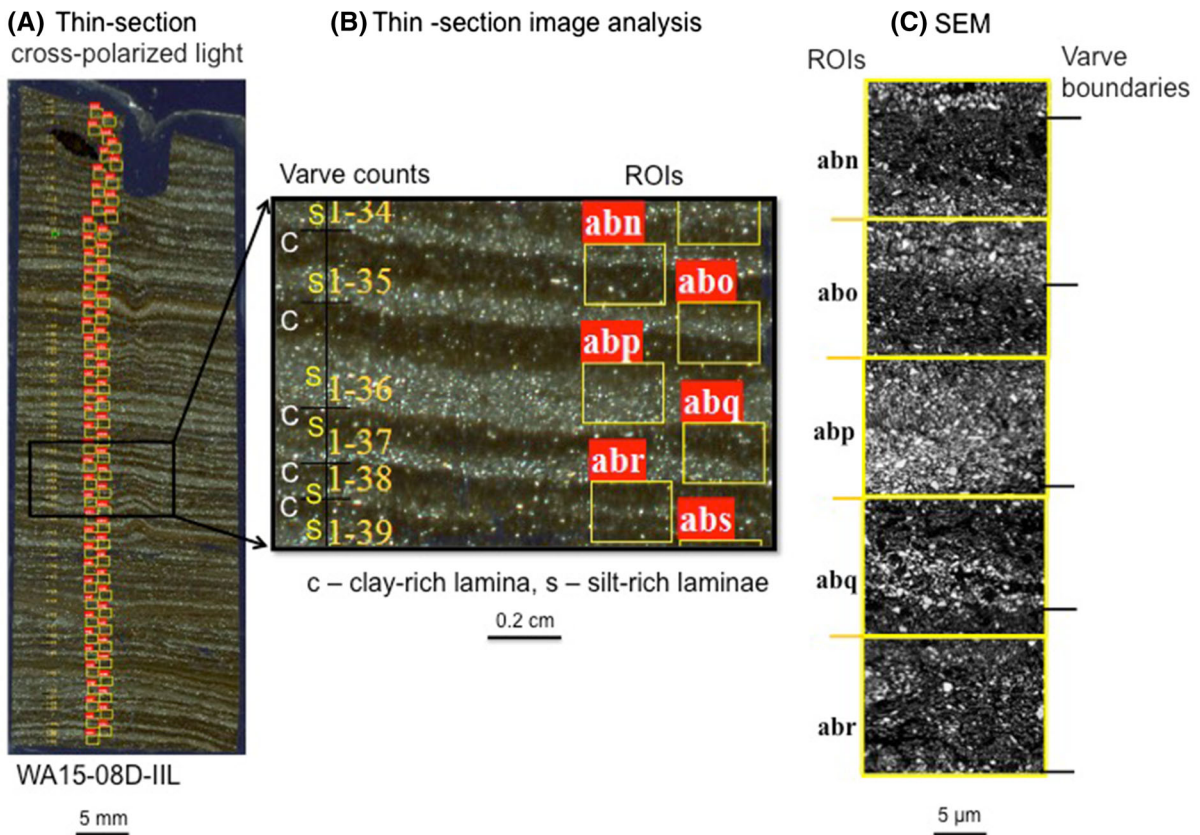
Fig. 2 Illustration of typical varve structure from Lake Walker, interpreted as clastic varves: **A** Flat-bed thin-section image showing **B** two main lithologic layers: clay-rich laminae (denoted as "c") deposited during winter and silt-rich laminae (denoted as "s") deposited between spring melt and autumn. Black horizontal bars indicate varve boundaries while numbers indicate varve counts (not in years). Regions of interest (ROIs) are shown at the right side lettered squares. **C** SEM images related to ROIs (as shown in B). SEM images show relatively clear contrast between clayey and silty laminae (letters and yellow squares indicate ROI boundaries, while black horizontal lines indicate varve boundaries

Table 3 Univariate statistics of the physical parameters analysed using PAST software from the composite core WA15-08-U ($\sim$ 175 to 263 cm cd) Lake Walker

	VT	mD_0	sD_0	$minD_0$	$maxD_0$	$P75\_D_0$	$P90\_D_0$	$P95\_D_0$	$P98\_D_0$	$P99\_D_0$
N	923	923	923	923	923	923	923	923	923	923
Min	0.169	5.171	2.736	3.568	16.622	7.047	9.305	11.17	13.729	14.936
Max	7.620	9.271	6.945	3.568	109.645	13.446	19.278	24.067	32.047	37.701
Mean	0.861	6.378	4.265	3.568	31.758	9.483	13.211	16.094	19.889	22.566
Std. error	0.018	0.020	0.021	2.35E-15	0.264	0.030	0.047	0.063	0.087	0.107
VAR	0.289	0.380	0.414	5.12E-27	64.232	0.848	2.053	3.648	7.053	10.594
SD	0.537	0.616	0.643	7.15E-14	8.015	0.921	1.433	1.910	2.656	3.255

VT, varve thickness (mm); VAR, Variance; SD, Standard deviation

Table 4 Spearman's rank correlation of varve thickness and grain size parameters from the composite core WA15-08-U (175–262.5 cm cd), Lake Walker

VT	mD_0	sD_0	$maxD_0$	$P75 D_0$	$P90\_D_0$	$P95\_D_0$	$P98\_D_0$	$P99\_D_0$
r_s	0.1944	0.1929	0.1586	0.2184	0.2035	0.2042	0.166	0.1713
p value	0.0001	0.0001	0.0001	0.0001	0.0001	0.0001	0.0001	0.0001

VT, Varve thickness; r_s, Spearman's rank correlation coefficient

179 cm cd dated 2361 ± 5 cal BP (Table 2) (discussed below).

Laminae couplet counts using thin-section and image analysis

Laminae couplet counts by two different researchers summed to 901 "varves" (O.P.N) and 923 varves (F.L) within this interval (Fig. 3C). The difference between the two individual counts (O.P.N and F.L) ranged from ± 1 to ± 12 varve years per thin section, with a total difference of approximately ± 22 years for the entire test interval (175–263 cm cd). The error in counting ranges from ~ 0.1 to $\sim 1.5\%$ (Fig. 3C).

Laminae visibility and counting, XRF data

The composite core WA15-08-U (0–352 cm cd) comprises mainly laminated and partially laminated sediments (Nzekwe et al. 2018) (Fig. 2, ESMs 2, 3). The laminations observed are generally horizontal and continuous (Fig. 2A, B). Their "Lamination visibility index" (LVI) (Nzekwe et al. 2018) is between 2 and 4 (visible to distinct) over the entire interval. Within the selected interval (~ 175 to 263 cm cd; Fig. 4B–D), the laminations appear clear to distinct (LVI: 3–4).

Downcore XRF data for selected elements (Ti, K, Zr) on core WA15-08-U (~ 0–360 cm cd) is shown in Fig. 5. The lower part of the core is characterized by relatively steady and regular elemental variations compared to the upper part of the core that is characterized by a generally decreasing upward profile of the selected elements.

Manual counting of laminae couplets using PeakCounter

An illustration of laminae counting on the selected interval of core WA15-08-U (175–263 cm cd) using PeakCounter is shown on Fig. 6. Specifically, gray scale value from the ITRAX radiograph and five selected XRF elements (Fe, K, Si, Ti and the inc/coh ratio) with traceable concentrations were overlapped and compared within an active window (selected interval) within the core (Fig. 6). As shown in Table 5, a total of 561 laminae couplets were counted within the 175–263 cm cd interval of core WA15-08-U which includes: 356 "VQI 1", 183 "VQI 2", 22 "VQI 3", and 0 "VQI 4" (laminae couplets) counts. The rapidly deposited layers (ESM 5) were excluded from the PeakCounter varve count (shown as breaks in the grey line, Fig. 3C). However, there was no sign of erosion below each of these RDL based on CT-scans and SEM images.

Statistical analysis of elemental data

Results of principal component analysis (PCA) of XRF elements from core WA15-08-U reveal XRF elemental associations and possible sources of sediments (Fig. 7, ESMs 6, 7). The eigenvalue of the first five components are higher than the Joliffe cut-off (0.7) respectively, which indicates these components appear significant (ESM 6A). However, the broken stick line (ESM 6B) indicates that the first component explains 40% of the variance (red line) (Hammer et al. 2001). PCA loadings for the first principal components show two groups: positive loadings (Si, K, Ca, Ti, Zn, Rb, Ni, Zr) and negative loadings (Mn, Fe, and inc/coh) (ESM 7). The PCA scatter plot for PC1 reveals four associations: (1) Si, Ti, K, Ca, Zr, Ni and Zn; (2): Mn and Fe; (3): inc/coh, and (4): Cl (Fig. 7).

Annual μ-XRF and grain-size variability between ~ 3230 and 2320 BP

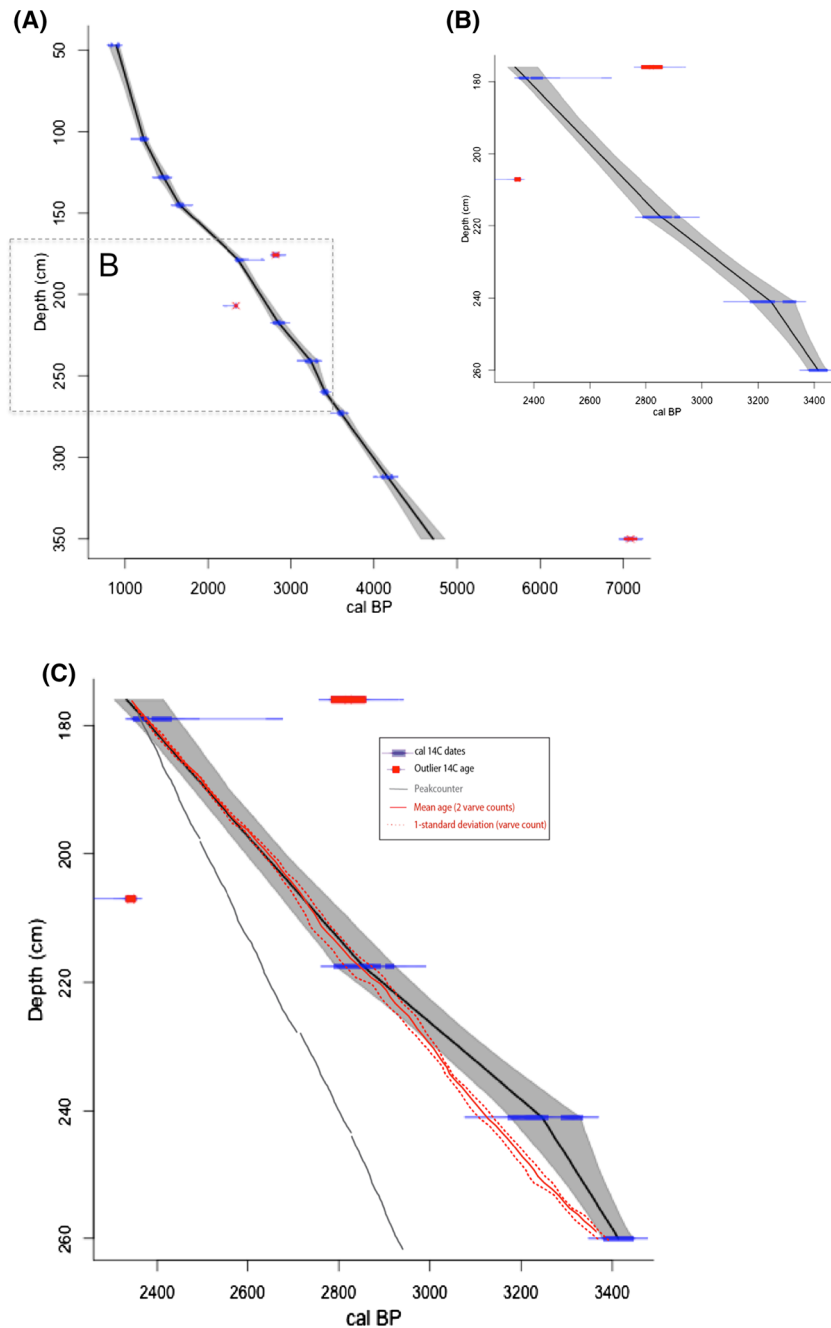Most of the μ-XRF elements exhibit similar variability during the interval under study (Fig. 8). The Zr and

Fig. 3 A Age-depth model of the composite core WA15-08-U (∼50 to 350 cm composite depth, cd) from Lake Walker based on radiocarbon dating. The model is constrained by ten dates (shown in blue colour), with three other dates as outliers (shown in red colour). The outliers were sampled at 176, 207 and 350 cm cd, and derived from bulk sediment (Table 3). The insert **B** shows the age-depth model of the section of core WA15-08-U (∼ 175 to 263 cm cd) that was analyzed for varve

occurrence. The grey shading represents the 95% confidence interval calculated by Clam (Blaauw 2010a). **C** Comparison of age-depth models for the laminated interval of core WA15-08-U (∼ 175 to 263 cm cd) based on AMS ^{14}C dating (**B**), semi-automatic counting using PeakCounter software (Marshall et al 2012); two individual varve counts based on thin-sections in this study (O.P.N and F.L); and the mean varve count by the two researchers

grain-size data show an increasing trend from the earlier part of the sequence and culminating around 2.7 ka cal BP. CT-scan (Hounsfield Unit: HU) reveals similar variability compared to the μ-XRF throughout the interval of interest, including higher relative density from 2800 to 2600 BP. Both Zr and the 99th percentile (P99D$_0$) depict strong co-variability throughout their overlapping period (Fig. 8, ESM 8).

Discussion

Chronology and radiometric dating

The chronology of recent sedimentation (deposited during the last ∼ 150 years) in Lake Walker was established by ^{210}Pb and ^{137}Cs dating (Nzekwe et al. 2018). The radiocarbon-based age-depth model (Fig. 3A) of core WA15-08-U (∼ 0 to 350 cm cd) is constrained by ten radiocarbon ages, while 3 ages are considered as outliers (176, 207 and 350 cm cd; Fig. 3A, B). Age reversals are common issues when dating bulk sediments in the absence of datable macrofossils (Grimm et al. 2009), which appears to be the case for our three outlier samples. Two of the outliers (at 176 and 207 cm cd) are located near the depth interval (between 176 and 179 cm cd) where there is an age reversal (Blaauw 2010a). These samples were sampled near the (∼ 5 cm) edge of the individual core sections that make up the composite sequence (Tables 1, 2), where some disturbance, and possible contamination can occur. The older outlying dates at 176 cm cd could be attributed to the dating of reworked bulk sediment material, while the occurrence of the younger date (at 207 cm cd) suggests possible contamination during sediment deposition and/or laboratory analysis (Butler et al. 2004; Hajdas et al. 1995). However, the lowermost outlier (at 350 cm cd) is likely caused by the dating of material from a relatively thick lamina, described as a rapidly deposited layer (St-Onge et al. 2007, 2012), which might have preserved older remobilised sediments (Gagnon-Poiré et al. 2019). However, as shown in Fig. 3A (and Table 2), the fact that the age of the two (2) wood fragments, at 128 and 179 cm cd (which are more reliable than bulk sediments) fit in a linear relationship with the ages of eight (8) bulk sediment-derived ages indicates that the radiocarbon age-depth model is robust, despite the exclusion of three (3)

outlier dates. Hence, the varve chronology from the selected interval of the composite core WA15-08-U (175–263 cm cd) that is anchored on four radiocarbon dates that range from 3230 to 2320 ± 20 cal BP, is also reliable (Fig. 3B, C).

Comparison of varve counting methods and error estimates

The varve chronology constructed using manual counts from the PeakCounter software does not match with the chronologies constructed from individual counts from thin sections and the AMS ^{14}C ages from within the counted interval for the selected interval of the composite sequence (175–263 cm cd) (Fig. 3C). More specifically, the varve chronology model constructed using PeakCounter has a steeper slope compared to the chronology constructed from individual thin-section counts, and plots progressively away from the radiocarbon age-depth model. However, the varve chronology model from thin-section counts has a gentler gradient and correlates closely with the radiocarbon age-depth model (Fig. 3C). The mean varve count from the thin section (red line; Fig. 3C) depicts the average of the individual counts by two independent researchers (O.P.N and F.L). The difference between the two counts (O.P.N and F.L) and the mean varve count defines the standard deviation of the varve chronology (Fig. 3C, Table 3).

The difference in varve counts between the varve chronologies established using the PeakCounter software and thin-section ranges from ± 5 to ∼ 350 varve years (Fig. 3C), which corresponds to an error of ± 40%. As noted already, error in individual laminae counts (O.P.N and F.L) using thin-section ranges from ∼ 0.1 to ∼ 1.5%. For PeakCounter, the VQI was used to estimate the error (counts by O.P.N only) based on maximum standard deviation of counts per VQI index. The VQI level 1 (with 356 counts out of 561 total counts) accounted for the maximum deviation, which indicates that the majority of counted varves were "faint". In summary, the varve chronology established from the thin sections is interpreted to be more reliable than that from the PeakCounter because it more closely follows the AMS [14]C (Fig. 3C).
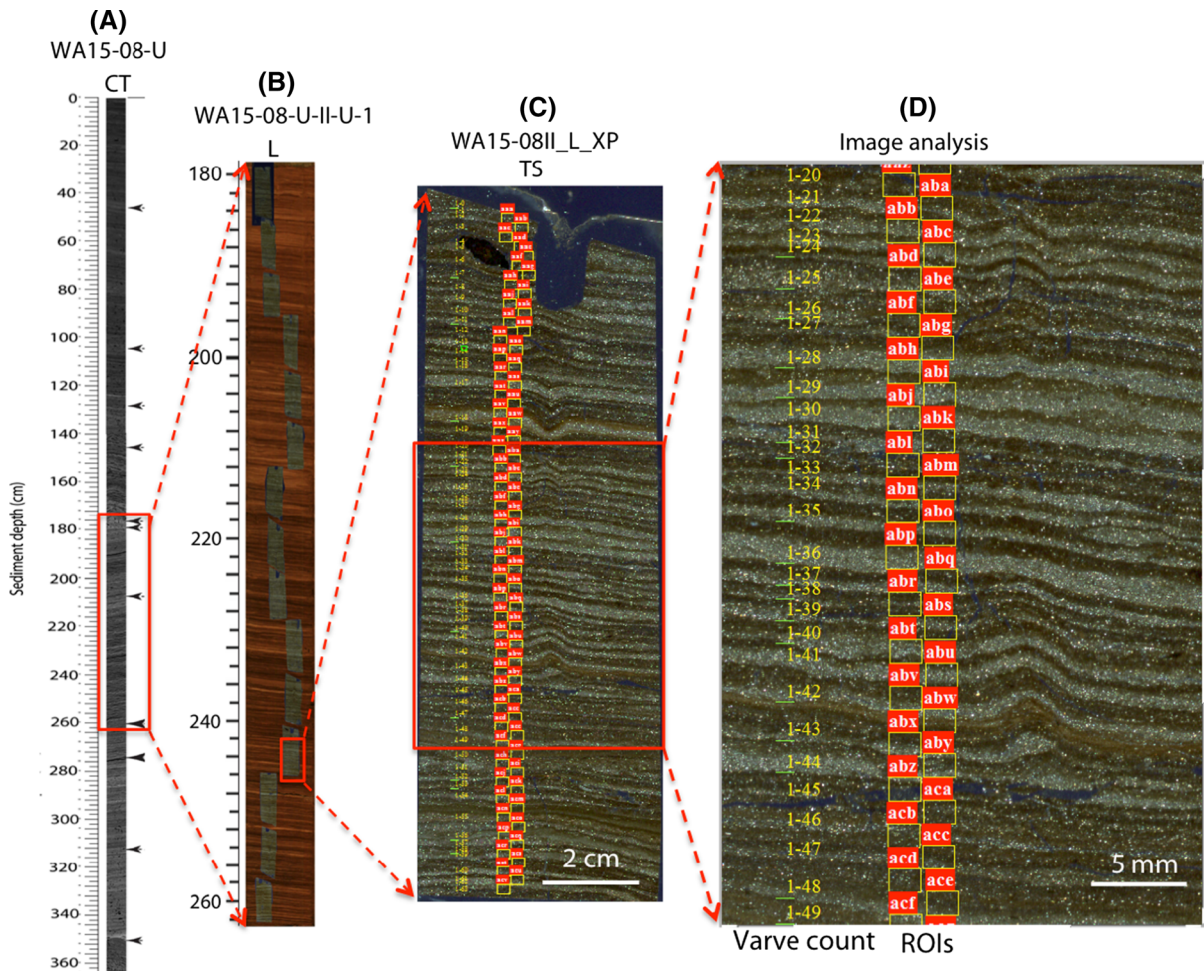
Fig. 4 Illustration of multi-scale image analyses of the composite core WA15-08-U (Lake Walker) to select a laminated interval and establish a varve record: **a** CT-scan of the upper ~ 4 m part of the core to delineate laminated intervals (black arrows indicate depths sampled for ^14C dating; **b** Line-scan image of a selected interval with regular laminations; **c** Thin-section from the selected interval showing laminae with clear-distinct boundaries; **d** Image analysis of varve counts and selection of regions of interests for particle size analysis using SEM

Laminae formation and preservation

Favourable conditions for the deposition of varved sediments in clastic environments include: a seasonally contrasted sedimentary supply, adequate sedimentation rates, seasonal or permanent anoxia, and a relatively deep basin (O'Sullivan 1983; Larsen and MacDonald 1993; Larsen et al. 1998; Schnurrenberger et al. 2003; Tylmann et al. 2012; Jenny et al. 2013; Zolitschka et al. 2015; Nzekwe et al. 2018). Varves from Lake Walker can be classified into the clastic varves category of Zolitschka et al (2015): a fine silt layer is deposited between spring melt and autumn, is overlain by clay-rich layer deposited during winter

(Fig. 2), which typically lasts for 5 months, from December to April (Nzekwe et al. 2018). The fine silt-rich layer is richer in elements usually interpreted as indicators of a detritic input (Si, Ti and Rb), while the clay-rich layer is richer in Fe and Mn, as observed elsewhere in clastic varves (Cuven et al. 2010).

PCA scatter plots of annually resolved XRF data (Fig. 7) indicates that the input is probably linked to silicates and carbonates (Rothwell and Croudace 2015). Detritic influence is predominant during the period of 2300 to 2800 BP, particularly during the interval 2700–3000 BP (Fig. 7). The closer association of inc/coh with Mn and Fe and divergent association with Ti and K (Fig. 7) suggests that
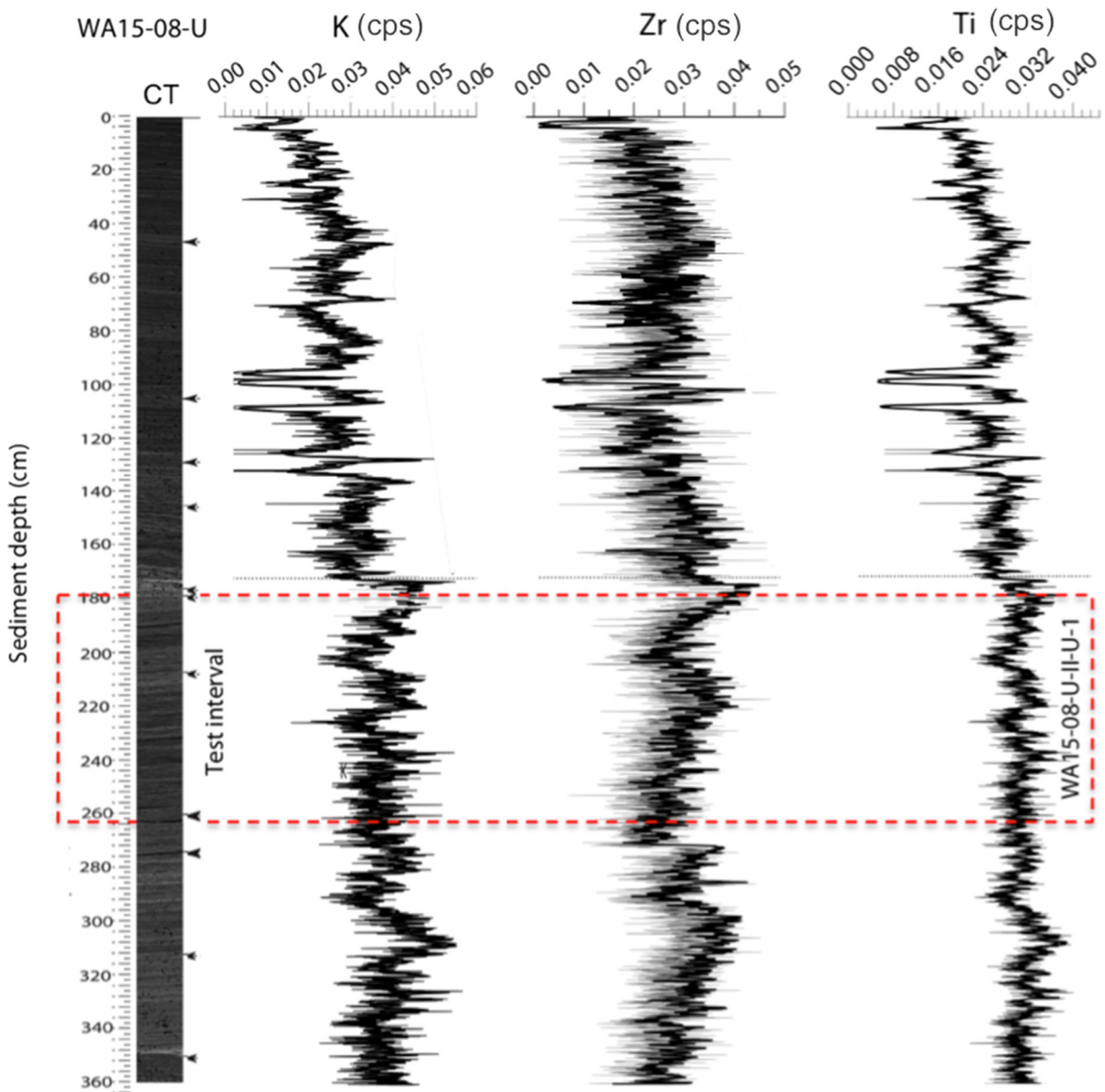
Fig. 5 XRF data for the composite core WA15-08-U showing CT-scan frontal view (CT) and vertical profiles of selected elements along the core. The number of counts for each element in a spectrum acquired for a specific depth interval was normalized by the total number of counts of that spectrum (expressed in counts per second, cps). Elemental variations are relatively more regular in the lower part of the core compared to the upper part, where they show general upward reduction. For preliminary attempts to establish a varve chronology, the middle part of the core (∼ 175 to 263 cm cd) was selected for analysis using PeakCounter software

organic matter preferentially bounds with fine sediments that are deposited under the ice in an oxygen-limited water column (Rothwell and Croudace 2015).

This study demonstrated that Lake Walker contains laminated and varved intervals during the period 3230 to 2320 ± 20 cal BP, and that the preservation of varved sediments generally improves with increasing depth in the composite core, as shown in Fig. 9. This observation is similar to a study by Kinder et al. (2013). The error limits in varve counting decreases with increasing depths, suggesting improved laminae preservation (Nzekwe et al. 2018; Tylmann et al.
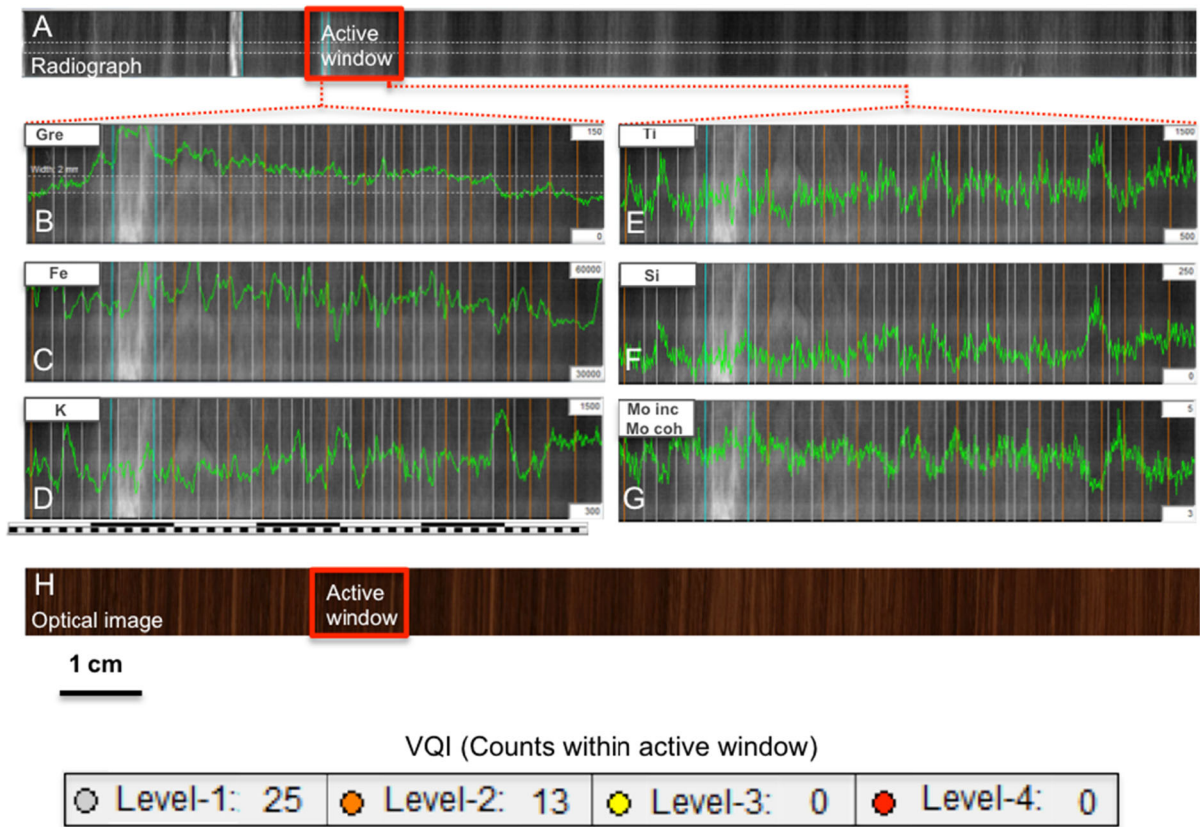
Fig. 6 Illustration of the multi-parameter approach using the PeakCounter Software (Marshall et al. 2012) for lamina/varve counts on core WA15-08-U (Lake Walker). Parameters include: **A** Radiograph (top) and optical image (below, **H**) of the core section (~ 175 to 263 cm cd). (Middle) For an active window (see radiograph), grey scale and XRF elements (Fe, K, Ti, Si, inc/coh ratio) are overlapped (**B–G**), where vertical marked lines represent laminations labelled based on varve quality index, with level 1 representing the lowest quality of varve, and level 4 representing the highest quality (Table 5)

Table 5 Summary data of varve counts on a section of the composite core WA15-08-U (~ 175 to 263 cm cd) using the PeakCounter software (Marshall et al. 2012)

Composite depth (cm cd)	VQI 1	VQI 2	VQI 3	VQI 4	Total
175–240	264	148	22	0	434
240–241	2	0	0	0	2
241–246	19	15	0	0	34
246–263	71	20	0	0	91
Whole interval	356	183	22	0	561

Level 1, 2, 3, 4 represent the varve quality indices used, with level 1 representing the lowest quality of varve, and level 4 representing the highest quality

2012; Zolitschka et al. 2015), which is possibly due to favourable morphological factors such as higher relative depth, anoxia and less sediment mixing potential (Larsen and MacDonald 1993; Larsen et al. 1998). Also, the LVI and VQI improve with increasing depth, while varve composition remains principally clastic at all depths (Fig. 9).
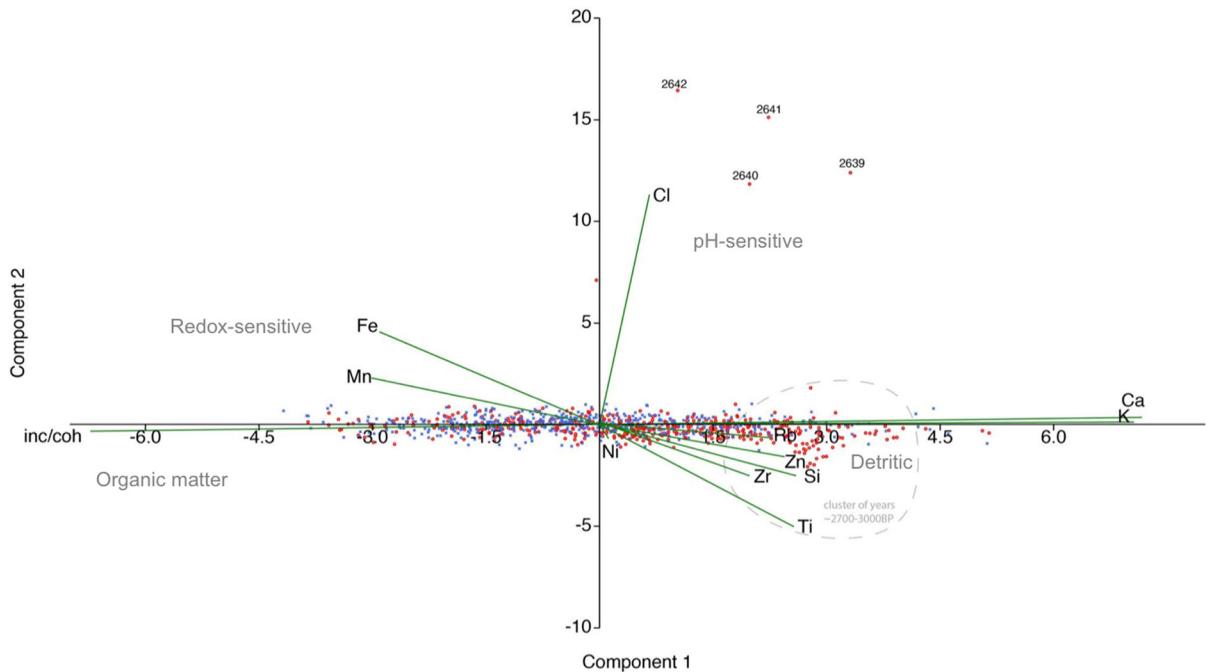
Fig. 7 PCA scatter plots of annually resolved XRF data (PC1, ESM 7). The red dots represent years 2300-2800 BP whereas blue dots are years after 2800BP. In general, the years 2300-2800 BP are characterized by more detritic influence, particularly during the interval 2700-3000 BP

Comparison with other lacustrine records in eastern Canada

Sedimentation rate in Lake Walker during the last $\sim$ 3.5 ka cal BP ranged from 0.4 to 1.75 mm a^{-1}. Such sedimentation rates are comparable to those in lakes within the central and southern regions of the province of Québec, for example, in Lake Jacques-Cartier: 0.40 mm a^{-1} (Philibert 2012); Lake Yasinki: 0.50 mm a^{-1} (Fortin et al. 2012); Lake Mékinac 0.18 mm a^{-1} (Trottier 2016); Lake Pasteur 0.04–0.87 mm a^{-1} (Nzekwe et al. 2018); Lake Pentecôte: 0.48–0.90 mm a^{-1} (Gagnon-Poiré et al. 2019; Nzekwe et al. 2018); Lake St-Joseph: 0.7 mm a^{-1} (Normandeau et al. 2013; Trottier et al. 2019), Lake Aux Sables: 0.8 mm a^{-1}, and Lake Maskinongé: 0.18 mm a^{-1} (Trottier et al. 2019), though no varves have been reported from these lakes. In general, the sediment accumulation rate of Lake Walker and other nearby lakes suggests that the regional sedimentation rate ranges from 0.4 to $\sim$ 2 mm a^{-1} (Table 6). A comparison of morphometric characteristics of the above-listed lakes is shown in Table 6.

In the Québec-Labrador region, the most similar reported varved site is Grand Lake, a fjord lake with maximum depth of 245 m (Table 6), located in Labrador, $\sim$ 600 km northeast of Lake Walker (Fortin et al. 2012; Gagnon-Poiré et al. 2021; Trottier et al. 2020). Although the reported average varve thicknesses are higher (between 1 to 5 mm) in proximal sites at Grand Lake, they are thinner in more distal cores (Gagnon-Poiré et al. 2021), and more importantly, the structure of these varves is similar to the ones found at Lake Walker. Moreover, the headwaters of the rivers feeding these two lakes are located in the same area, covered by a hilly boreal forest. It is then realistic to transpose the paleoenvironmental interpretation made at Grand Lake to Lake Walker. Gagnon-Poiré et al. (2021) found a strong correlation between the thickness and the grain size of detrital silty layer of the varves with the local instrumental hydrological record of the Naskaupi River (r = 0.68 and 0.75, respectively), and were able to reconstruct past mean and maximum annual discharge. They also showed that the record could be used as a proxy for regional river discharge conditions. The record at Grand Lake only extends back 160 years, but its qualitative
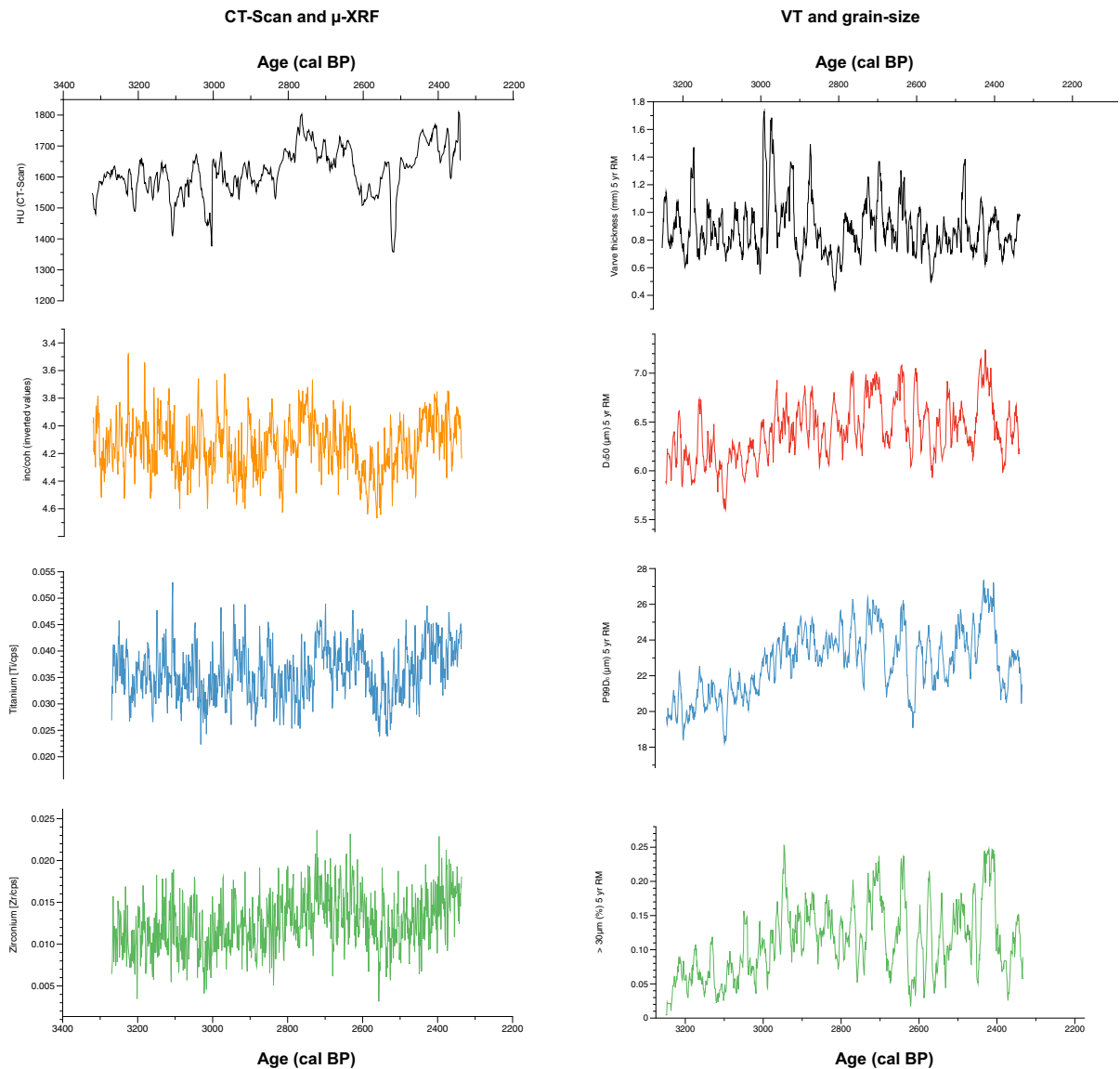
Fig. 8 Physical and geochemical properties for the Lake Walker from $\sim$ 3230 to 2330 BP. Left panel: CT scan Hounsfield Unit (HU), ratio inc/coh, Titanium (Ti), and Zirconium (Zr). Right panel: Varve thickness, the median grain-size (D050), the 99th percentile (P99D$_0$) and the fraction greater than 30 μm

interpretation of varve thickness and varve grain size can be applied to our older 900-yr-long varve records at Lake Walker since the paleogeographic conditions have not changed since then.

To mention, the late Holocene varves from Lake Walker are different both in age and laminae structure from glacial varves formed during the last deglaciation in eastern Canada. Glacial varves reported from Lake Walker (Gagnon-Poiré et al. 2019), Lake Barlow-Ojibway (Breckenridge et al. 2012), Lake Jacques-Cartier (Philibert 2012), the Deschaillons varves in the St. Lawrence Valley (Besré and Occhietti 1990), and varves from western Québec-northeastern Ontario (Brooks 2020) are marked by relatively thicker (> 1 cm) varves comprising predominantly clay.
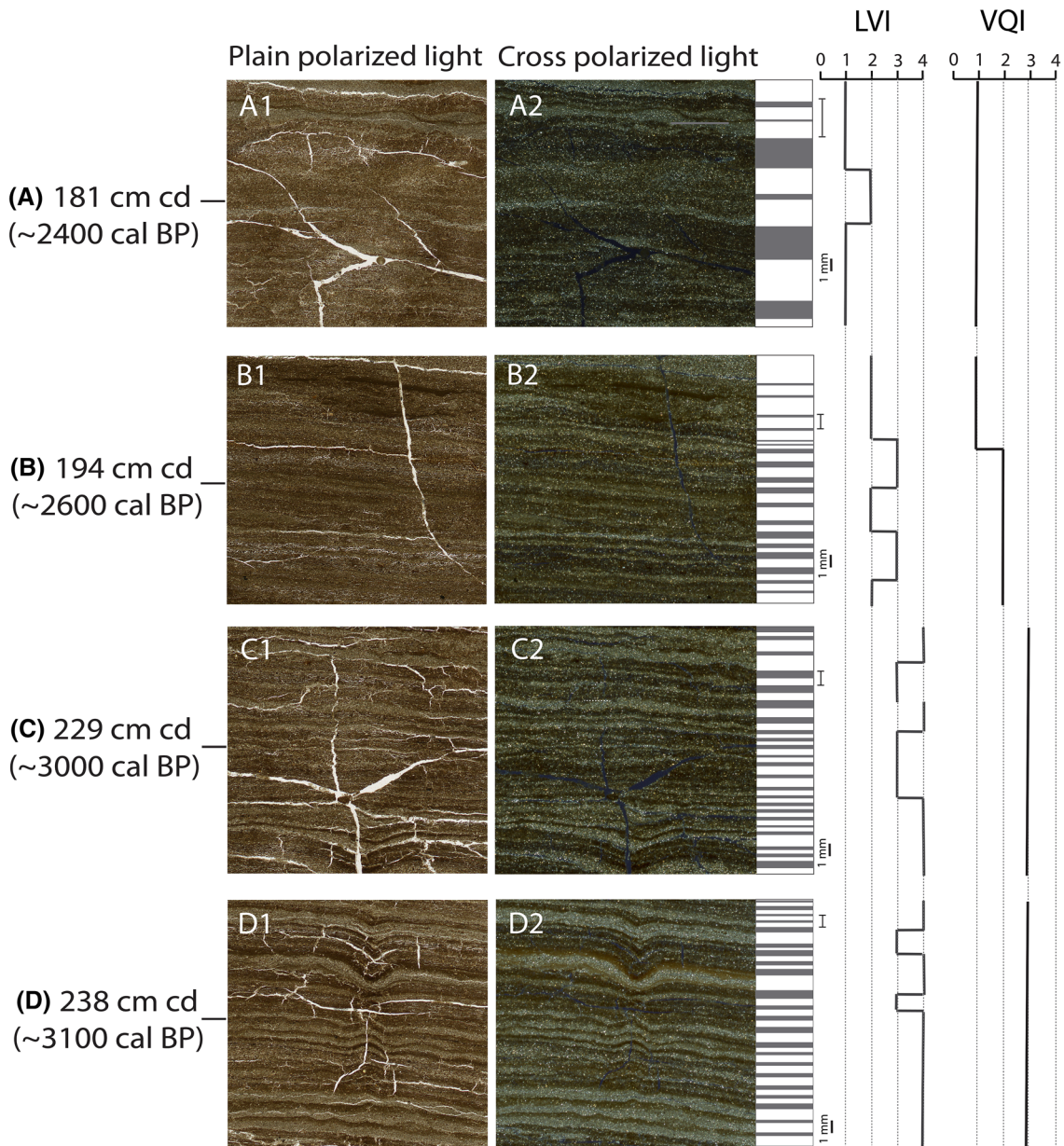
Fig. 9 Illustration of the varve structure ate four different depths of the composite core WA15-08-U from Lake Walker, which demonstrate that laminae visibility index (LVI) and varve quality index (VQI) improves with increasing sediment depth

Lake Walker varve record: prospects and challenges

Although laminae couplets on core WA15-08-U (Lake Walker) were generally visible on CT-scan images, line-scan photos and radiographs, however, it was more difficult to clearly delineate varve boundaries on them (mean varve thickness of 0.86 mm), because

their resolution were insufficient, i.e., 600 μm, 50 μm and 100 μm, respectively. Using the PeakCounter software for laminae counting proved to be unsuccessful here at adequately delineating laminae couplet boundaries (Fig. 6, ESM 6) because it relies on the ITRAX resolution that is 100 μm.

Possible sources of error associated with varve counting using PeakCounter in Lake Walker include:

Table 6 Comparison of lacustrine and morphometric data from some lakes in eastern Canada

Lake	Latitude (°N)	Longitude (°W)	Altitude (m asl)	Maximum depth (m)	Lake Area (km²)	Sedimentation rate (mm a⁻¹)	Coring depth (m)	References
Jacques-Cartier	47.585200	71.207300	795	67	12	0.40	2.5–55	Philibert (2012)
Yasinki	77.583056	53.278056	142	–	–	0.50	–	Fortin et al. (2012)
Mékinac	47.067000	72.683000	165	145	23	0.18	–	Trottier (2016)
Aux-Sables	46.898833	72.365833	150	41	5.2	0.80	39	Trottier et al. (2019)
Maskinongé	46.329667	73.398667	140	25	10.2	1.80	18.5	Trottier et al. (2019)
St-Joseph	46.916667	71.650000	160	37	11.3	0.5–0.7	37	Normandeau et al. (2013), Trottier et al. (2019)
Pasteur	50.217000	66.067000	86	70	19.3	0.04–0.87	71	Nzekwe et al. (2018)
Pentecôte	49.867000	67.333000	84	130	18.9	0.48–0.90	40	Nzekwe et al. (2018), Gagnon-Poiré et al. (2019)
Grand Lake*	53.690439	60.535147	15	245	150	0.50–0.1	93–176	Trottier et al. (2020), Gagnon-Poiré et al. (2021)
Walker*	50.267000	67.150000	115	271	41	0.65–0.95	∼ 140 to 150	Nzekwe et al. (2018); This study

Asl, Above sea level

(–) Data unreported

Coring depth refers to cores from which sedimentation rates were derived

*Lakes where varve records have been reported

(1) technical challenges such as image resolution with respect to very fine laminae thickness and/or detectable thresholds of XRF elements. Considering a modal and median varve thickness of 0.65 and 0.74 mm, respectively, it means that more than 50% of the laminations are represented by only 6 to 7 data points, which is an insufficient number for delineating a couplet; (2) subjectivity of delineation of laminations/varves by the analyst (Schlolaut et al. 2012); and (3) depositional events such as the presence of rapidly deposited layers (ESM 6), partial or incomplete laminations and low depositional rates (Zolitschka et al. 2015), as observed in Lake Walker.

On the contrary, thin-section and SEM images were more suitable to count varves due to their improved phase contrast and higher resolution (Figs. 2, 4) (Francus 2006; Francus and Karabanov 2000; Lapointe et al. 2012). Therefore, these images could provide the principal basis for counting laminations/varves from core WA15-08-U. Counting and measuring varves on SEM images were facilitated by

the use of an in-house software (Francus and Nobert 2007), allowing multiple counts by different researchers. However, possible sources of error associated with this counting technique include: (1) technical challenges such as cracks in sediments generated during resin embedding and freeze drying, and cutting successive thin sections with adequate (at least 1 cm) sediment overlap, and (2) depositional factors, as stated above.

Therefore, the quality of the laminations in our composite sequence was not sufficient to develop a robust continuous varved record over the entire length of the composite profile. It does not mean that a fully varved record does not exist at Lake Walker. Paleo-geographic conditions remained stable in the region since the last 6000 years, and sub-bottom profile survey revealed many other potential suitable coring sites devoid of disturbances (Gagnon-Poiré et al. 2019). Yet, a complete record most probably exists at a more proximal location in Lake Walker and, if the comparison with Grand lake is valid, laminations

should be thicker and hence easier to delineate. Nevertheless, it is possible to infer a paleoclimatic interpretation at low resolution for the entire record, with higher resolution for the 175–263 cm cd interval.

Paleoclimatic interpretation of Lake Walker record

The long-term μ-XRF dataset underscores an interval of relatively stable elemental variability from ∼ 360 to 170 cm, whereas a declining trend in elemental data (K, Zr, Ti) is observable from 170 cm to present (Fig. 5). This is consistent with the overall decrease of relative density values (CT-Scan) starting at ∼ 170 to 0 cm cd observed in the same core (Gagnon-Poiré et al. 2019). In addition, the radiocarbon age-depth model indicates an increase in sedimentation rates below ∼ 170 cm cd (Fig. 3A). Altogether, this suggests increased runoff conditions below 170 cm (around ∼ 2300 cal BP) and in the earlier part (deeper) of the composite sequence. Increased runoff is indicative of greater snow precipitation in winter.

Although there are few reconstructions of NAO that reach beyond our research interval/last 3200 yr BP, the grain-size evolution at Lake Walker strongly co-varies with a unique NAO from SW Greenland (Olsen et al. 2012). The Lake Walker record is averaged every 25 years to equal the reconstructed NAO temporal resolution, and this revealed a significant negative correlation (Fig. 11; r = − 0.77, p < 0.001). We note too that Titanium at Lake Walker is significantly correlated (r = − 0.48, p = 0.002) to this NAO, unlike the other proxies. Increasing trend in grain-size values from ∼ 3200 to 2800 cal BP that maximizes from 2800–2600 cal BP and from 2500 to 2400 cal BP is also seen in the other grain-size proxies and the Zr data (Fig. 8), possibly linked to periods of more persistent negative NAO (Fig. 10).

Cool conditions associated with increased ice rafted debris were recorded at ∼ 3300 to 2500 cal BP, coinciding with a long-lasting low solar activity that peaked around ∼ 2700 cal BP (Martin-Puertas et al. 2012; van Geel et al. 2000; Wanner et al. 2011). Several studies underline that reduction in solar irradiance can modify atmospheric pressure gradient, with a tendency to project onto the negative phase of the North Atlantic Oscillation (NAO) (Gray et al. 2013; Moffa-Sánchez et al. 2014).

To explore the possible connection between negative NAO and increased grain size at Lake Walker, investigating the winter precipitation anomalies during a similar period in the instrumental era would be desired. Lower Atlantic SSTs (Fig. 11B) along with negative NAO (Fig. 11A) occurred during 1976–1986, offering a possible analogy to the climatic context of ∼ 2800 years ago. Observational evidence indicates increased winter precipitation over most of Québec during this cool period, including the Lake Walker region (Fig. 11C). This positive precipitation anomaly would then have promoted enhanced spring runoff caused by greater snow accumulation, consistent with the documented higher fluxes at Grand Lake, in the Québec-Labrador region (Fig. 11C), from 1976 to 1986 (Gagnon-Poiré et al. 2021).

An anomalous period of drift ice and ice rafted debris occurred at about 2700 cal BP, and this inevitably contributed to the cooling of the North-Atlantic (Bond et al. 2001), as also observed in a recent reconstructed Atlantic SSTs (Lapointe et al. 2020). This period appears to have also been one of a persistent negative NAO (Martin-Puertas et al. 2012). The cause of the cooling of the North Atlantic in the mid 1970s to the 1980s is not fully understood, but strong evidence shows that increased sea ice export from Fram Strait during the 1960s certainly played a major role (Ionita et al. 2016). Based on both observational and paleo evidence (Figs. 10, 11), it is plausible that the increase in grain size described at Lake Walker some 2800 years ago was related to such North-Atlantic cooling anomaly, with linkages associated with persistent negative NAO.
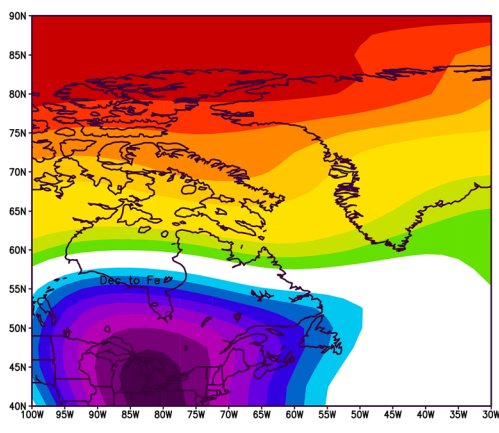
Conclusions

This study analysed laminated sediments from the composite core WA15-08-U (0–378 cm cd) collected from Lake Walker, Québec North Shore region, eastern Canada using multi-scale analyses of laminations/varves: CT-scan, μ-XRF, PeakCounter software and SEM image of thin sections. The main findings are as follows:

- Lake Walker likely holds a continuous annually laminated sediments record. The presence of varves in the best-preserved interval between ∼ 3230 to 2320 cal BP has been confirmed. Laminae
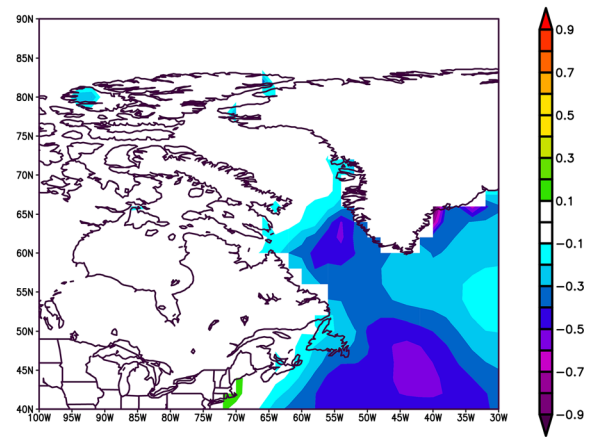
Fig. 10 North Atlantic Oscillation (NAO) compared to Lake Walker 99th percentile grain-size. Data at Lake Walker is resampled at the lowest resolution (25 years)
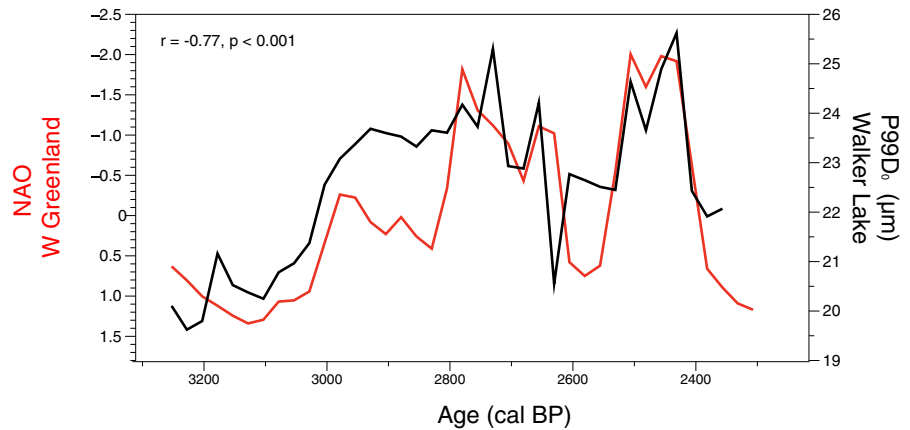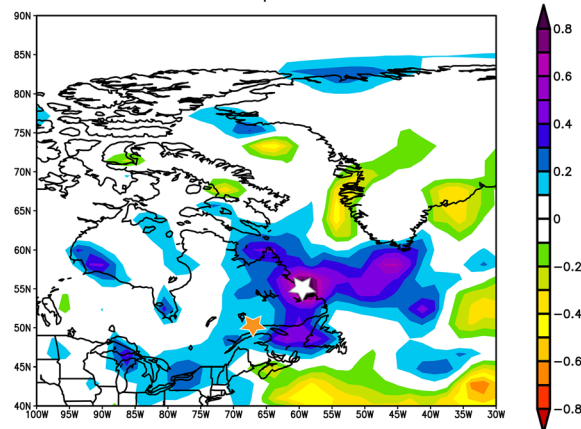

Fig. 11 A 500 hPa geopotential height (Kalnay et al. 2006) anomaly in the period of cooler Atlantic SSTs (1976–1986) compared to 1950–2000. The atmospheric pressure pattern is reminiscent of a negative NAO (A). **B** Same as **A**, but for sea surface temperature (SST) anomaly from the Extended Reconstructed SST (Huang et al. 2017). **C** Same as **B** but for precipitation rate (mm/day) from NCEP/NCAR. Orange and white stars denote Lake Walker and Grand Lake sites, respectively

preservation and varve quality generally improves with increasing depth.

- PeakCounter was not able to generate a robust chronology matching the AMS ^{14}C ages because laminations were too thin (mean varve thickness is 0.86 mm) and sometimes not distinct enough. However, the use of image analysis of thin-sections and SEM images allowed delineate and count varves to establish a floating chronology consistent with the radiocarbon dates.

- This new ~ 900-year floating varved chronology from Lake Walker, Québec North Shore region spans the interval ~ 3230 to 2320 cal BP. The record shows similarity with another low resolution NAO record in the region. Periods of synchronized cool Atlantic SSTs and negative phase NAO tend to coincide with greater snow accumulation in the region, thereby increasing grain size and sediment fluxes at Lake Walker.

- There is a high potential to establish a longer record from other laminated intervals from Lake Walker.

References

Arseneault D, Dy B, Gennaretti F, Autin J, Begin Y (2013) Developing millennial tree ring chronologies in the fire-prone North American boreal forest. J Quat Sci 28:283–292

Besré F, Occhietti S (1990) Les varves de Deschaillons, les rythmites du Saint-Maurice et les rythmites de Leclercville, Pleistocene supérieur, vallée du Saint-Laurent. Québec Geogr Phys Quatern 44:181–198

Blaauw M (2010a) Methods and code for 'classical' age-modelling of radiocarbon sequences. Quat Geochronol 5:512–518

Blaauw M (2010b) R-Code for 'classical' age-modelling (CLAM V1.0) of radiocarbon sequences. Supplement to: Blaauw, M (2010): Methods and code for 'classical' age-modelling of radiocarbon sequences Quaternary Geochronology, 5(5), 512-518. PANGAEA.

Boespflug X, Long BFN, Occhietti S (1995) Cat-scan in marine stratigraphy—a quantitative approach. Mar Geol 122:281–301

Bond G, Kromer B, Beer J, Muscheler R, Evans MN, Showers W, Hoffmann S, Lotti-Bond R, Hajdas I, Bonani G (2001) Persistent solar influence on North Atlantic climate during the Holocene. Science 294:2130–2136

Breckenridge A, Lowell TV, Stroup JS, Evans G (2012) A review and analysis of varve thickness records from glacial Lake Ojibway (Ontario and Quebec, Canada). Quat Int 260:43–54

Brooks GR (2020) Evidence of a strong paleoearthquake in ~ 9.1 ka cal BP interpreted from mass transport deposits, western Quebec–northeastern Ontario, Canada. Quat Sci Rev 234:106

Butler K, Prior CA, Flenley JR (2004) Anomalous radiocarbon dates from Easter Island. Radiocarbon 46:395–405

Centre d'expertise hydrique. (2016) Historique des données de différentes stations hydrométriques. Ministère de l'Environnement et de la Lutte contre les changements climatiques https://www.cehqgouvqcca/hydrometrie/historique_donnees/indexasp.

Cremer JF, Long B, Desrosiers G, de Montety L, Locat J (2002) Application of scanography to sediment density analysis and sediment structure characterization: Case of sediments deposited in the Saguenay River (Quebec, Canada) after the July 1996 flood. Can Geotech J 39:440–450

Croudace IW, Rindby A, Rothwell RG (2006) ITRAX: description and evaluation of a new multi-function X-ray core scanner. Spec Publ Geol Soc Lond 267:51

Cuven S, Francus P, Lamoureux SF (2010) Estimation of grain size variability with micro X-ray fluorescence in laminated lacustrine sediments, Cape Bounty, Canadian High Arctic. J Paleolimnol 44:803–817

Dodge Y (2003) The oxford dictionary of statistical terms. Oxford University Press, Oxford, p 506

Fortin D, Francus P, ARCHIVES Team (2012) Potentiel des sédiments lacustres annuellement laminés pour reconstruire les conditions hydroclimatiques au Québec-Labrador—Project ARCHIVES. Atelier du groupe ARCHIVES, Atelier Ouranos, Varennes, Québec

Fortin D, Francus P, Gebhardt AC, Hahn A, Kliem P, Lise-Pronovost A, Roychowdhury R, Labrie J, St-Onge G, Team PS (2013) Destructive and non-destructive density determination: method comparison and evaluation from the Laguna Potrok Aike sedimentary record. Quat Sci Rev 71:147–153

Francus P (1998) An image-analysis technique to measure grain-size variation in thin sections of soft elastic sediments. Sediment Geol 121:289–298

Francus P (2006) Image analysis, sediments and paleoenvironments. developments in paleoenvironmental research, vol 7. Springer, Dordrecht, p 330

Francus P, Asikainen CA (2001) Sub-sampling unconsolidated sediments: a solution for the preparation of undistorbed thin-sections from clay-rich sediments. J Paleolimnol 26:323–326

Francus P, Karabanov E (2000) A computer-assisted thin-section study of Lake Baikal sediments: a tool for understanding sedimentary processes and deciphering their climatic signal. Int J Earth Sci 89:260–267

Francus P, Nobert P (2007) An integrated computer system to acquire, process, measure and store images of laminated sediments. In: 4th international limnogeology congress, Barcelona, Spain (11–14th July)

Francus P, Bradley RS, Lewis T, Abbott M, Retelle M, Stoner JS (2008) Limnological and sedimentary processes at Sawtooth Lake, Canadian High Arctic, and their influence on varve formation. J Paleolimnol 40:963–985

Francus P, Ridge JC, Johnson MD (2013a) The Rise of Varves. GFF 135:229–230

Francus P, Von Suchodoletz H, Dietze M, Donner RV, Bouchard F, Roy AJ, Fagot M, Verschuren D, Kropelin S (2013b) Varved sediments of Lake Yoa (Ounianga Kebir, Chad) reveal progressive drying of the Sahara during the last 6100 years. Sedimentology 60:911–934

Gagnon-Poiré A, Lajeunesse P, Normandeau A, Francus P, St-Onge G, Nzekwe OP (2019) Corrigendum to "Late-Quaternary glacial to postglacial sedimentation in three adjacent fjord-lakes of the Québec North Shore (eastern Canadian Shield)"[Quat. Sci. Rev. 186 (2018) 91–110]. Quat Sci Rev 220:401–403

Gagnon-Poiré A, Brigode P, Francus P, Fortin D, Lajeunesse P, Dorion H, Trottier A-P (2021) Reconstructing past hydrology of eastern Canadian boreal catchments using clastic varved sediments and hydro-climatic modelling: 160 years of fluvial inflows. Clim Past 17:653–673

Gray LJ, Scaife AA, Mitchell DM, Osprey S, Ineson S, Hardiman S, Butchart N, Knight J, Sutton R, Kodera K (2013) A lagged response to the 11 year solar cycle in observed winter Atlantic/European weather patterns. J Geophys Res Atmos 118:13,405-413,420

Hajdas I, Zolitschka B, Ivy-Ochs SD, Beer J, Bonani G, Leroy SA, Negendank JW, Ramrath M, Suter M (1995) AMS radiocarbon dating of annually laminated sediments from Lake Holzmaar. Germany Quat Sci Rev 14:137–143

Hammer Ø, Harper DAT, Ryan PD (2001) Past: Paleontological Statistics Software Package for education and data analysis Paleontol. Electron 4:1–75

Ionita M, Scholz P, Lohmann G, Dima M, Prange M (2016) Linkages between atmospheric blocking, sea ice export through Fram Strait and the Atlantic Meridional Overturning Circulation. Sci Rep 6:1–10

Jenny J-P, Arnaud F, Dorioz J-M, Giguet Covex C, Frossard V, Sabatier P, Millet L, Reyss J-L, Tachikawa K, Bard E (2013) A spatiotemporal investigation of varved sediments highlights the dynamics of hypolimnetic hypoxia in a large hard-water lake over the last 150 years. Limnol Oceanogr 58:1395–1408

Kinder M, Tylmann W, Enters D, Piotrowska N, Poręba G, Zolitschka B (2013) Construction and validation of calendar-year time scale for annually laminated sediments–an example from Lake Szurpiły (NE Poland). GFF 135:248–257

Lajeunesse P (2014) Buried preglacial fluvial gorges and valleys preserved through Quaternary glaciations beneath the eastern Laurentide Ice Sheet. Geol Soc Am Bull 126:447–458

Lamoureux SF (1994) Embedding unfrozen lake sediments for thin section preparation. J Paleolimnol 10:141–146

Lapointe F, Bradley RS, Francus P, Balascio NL, Abbott MB, Stoner JS, St-Onge G, De Coninck A, Labarre T (2020) Annually resolved Atlantic sea surface temperature variability over the past 2,900 y. Proc Natl Acad Sci 117:27171–27178

Lapointe F, Francus P, Lamoureux SF, Said M, Cuven S (2012) 1750 years of large rainfall events inferred from particle size at East Lake, Cape Bounty, Melville Island, Canada. J Paleolimnol 48:159–173

Lapointe F, Francus P, Lamoureux SF, Vuille M, Jenny J-P, Bradley RS (2017) Influence of North Pacific decadal variability on the western Canadian Arctic over the past 700 years. Clim past 13:411–420

Lapointe F, Francus P, Stoner JS, Abbott MB, Balascio NL, Cook TL, Bradley RS, Forman SL, Besonen M, St-Onge G (2019) Chronology and sedimentology of a new 2.9 ka annually laminated record from South Sawtooth Lake, Ellesmere Island. Quat Sci Rev 222:105

Larsen CPS, MacDonald GM (1993) Lake morphometry, sediment mixing and the selection of sites for fine resolution palaeoecological studies. Quat Sci Rev 12:781–792

Larsen CPS, Pienitz R, Smol JP, Moser KA, Cumming BF, Blais JM, Macdonald GM, Hall RI (1998) Relations between lake morphometry and the presence of laminated lake sediments: A re-examination of Larsen and Macdonald (1993). Quat Sci Rev 17:711–717

Marshall M, Schlolaut G, Nakagawa T, Lamb H, Brauer A, Staff R, Ramsey CB, Tarasov P, Gotanda K, Haraguchi T, Yokoyama Y, Yonenobu H, Tada R (2012) A novel approach to varve counting using µXRF and X-radiography in combination with thin-section microscopy, applied to the Late Glacial chronology from Lake Suigetsu, Japan. Quat Geochronol 13:70–80

Martin-Puertas C, Matthes K, Brauer A, Muscheler R, Hansen F, Petrick C, Aldahan A, Possnert G, Van Geel B (2012) Regional atmospheric circulation shifts induced by a grand solar minimum. Nat Geosci 5:397–401

Moffa-Sánchez P, Born A, Hall IR, Thornalley DJ, Barker S (2014) Solar forcing of North Atlantic surface temperature and salinity over the past millennium. Nat Geosci 7:275

Nakagawa T, Gotanda K, Haraguchi T, Danhara T, Yonenobu H, Brauer A, Yokoyama Y, Tada R, Takemura K, Staff RA, Payne R, Bronk Ramsey C, Bryant C, Brock F, Schlolaut G, Marshall M, Tarasov P, Lamb H (2012) SG06, a fully continuous and varved sediment core from Lake Suigetsu, Japan: stratigraphy and potential for improving the radiocarbon calibration model and understanding of late Quaternary climate changes. Quat Sci Rev 36:164–176

Naulier M, Savard MM, Begin C, Marion J, Arseneault D, Begin Y (2014) Carbon and oxygen isotopes of lakeshore black spruce trees in northeastern Canada as proxies for climatic reconstruction. Chem Geol 374:37–43

Nicault A, Boucher E, Begin C, Guiot J, Marion J, Perreault L, Roy R, Savard MM, Begin Y (2014) Hydrological reconstruction from tree-ring multi-proxies over the last two

centuries at the Caniapiscau Reservoir, northern Quebec, Canada. J Hydrol 513:435–445

Normandeau A, Lajeunesse P, Philibert G (2013) Late-Quaternary morphostratigraphy of Lake St-Joseph (southeastern Canadian Shield): evolution from a semi-enclosed glacimarine basin to a postglacial lake. Sediment Geol 295:38–52

Normandeau A, Lajeunesse P, Poiré AG, Francus P (2016) Morphological expression of bedforms formed by supercritical sediment density flows on four fjord-lake deltas of the south-eastern Canadian Shield (Eastern Canada). Sedimentology 63:2106–2129

Nzekwe OP, Francus P, St-Onge G, Lajeunesse P, Fortin D, Gagnon-Poiré A, Philippe ÉGH, Normandeau A (2018) Recent sedimentation in three adjacent fjord-lakes on the Québec North Shore (eastern Canada): facies analysis, laminae preservation, and potential for varve formation. Can J Earth Sci 55:138–153

O'Sullivan PE (1983) Annually-laminated lake sediments and the study of Quaternary environmental changes—a review. Quat Sci Rev 1:245–313

Ojala AEK, Francus P, Zolitschka B, Besonen M, Lamoureux SF (2012) Characteristics of sedimentary varve chronologies—a review. Quat Sci Rev 43:45–60

Ojala AEK, Kosonen E, Weckstrom J, Korkonen S, Korhola A (2013) Seasonal formation of clastic-biogenic varves: the potential for palaeoenvironmental interpretations. GFF 135:237-U212

Olsen J, Anderson NJ, Knudsen MF (2012) Variability of the North Atlantic Oscillation over the past 5,200 years. Nat Geosci 5:808

Philibert G (2012) Évolution tardi-quaternaire du lac Jacques-Cartier, Reserve faunique des Laurentides, Québec. Mémoire de Maitrise en sciences géographiques, Département de Géographie, Faculté de Foresterie, de Geographie and Géomatique. Université Laval, Québec, p 113

Reimer PJ, Bard E, Bayliss A, Beck JW, Blackwell PG, Ramsey CB, Buck CE, Cheng H, Edwards RL, Friedrich M (2013) IntCal13 and Marine13 radiocarbon age calibration curves 0–50,000 years cal BP. Radiocarbon 55:1869–1887

Rothwell RG, Croudace IW (2015) Twenty years of XRF core scanning marine sediments: What do geochemical proxies tell us? In: Croudace IW, Rothwell RG (eds) Micro-XRF Studies of Sediment Cores, Developments in Paleoenvironmental Research 17. Springer, Dordrecht, pp 25–102

Schlolaut G, Marshall MH, Brauer A, Nakagawa T, Lamb HF, Staff RA, Bronk Ramsey C, Bryant CL, Brock F, Kossler A, Tarasov PE, Yokoyama Y, Tada R, Haraguchi T (2012) An automated method for varve interpolation and its application to the Late Glacial chronology from Lake Suigetsu Japan. Quat Geochronol 13:52–69

Schnurrenberger D, Russell J, Kelts K (2003) Classification of lacustrine sediments based on sedimentary components. J Paleolimnol 29:141–154

St-Onge G, Mulder T, Francus P, Long B (2007) Continuous physical properties of cored marine sediments. Proxies in Late Cenozoic Paleoceanography Elsevier, pp 63–98

St-Onge G, Chapron E, Mulsow S, Salas M, Viel M, Debret M, Foucher A, Mulder T, Winiarski T, Desmet M (2012) Comparison of earthquake-triggered turbidites from the Saguenay (Eastern Canada) and Reloncavi (Chilean margin) Fjords: Implications for paleoseismicity and sedimentology. Sediment Geol 243:63–107

Trottier A-P (2016) Les enregistrements sédimentaires tardiquaternaires de la paléosismicité dans les lacs Maskinongé, Mékinac, aux-Sables et Saint-Joseph (centre-sud du Québec). Mémoire de Maitrise en sciences géographiques, Département de Géographie, Faculté de Foresterie, de Geographie and Géomatique. Université Laval, Québec, p 85

Trottier A-P, Lajeunesse P, Normandeau A, Gagnon-Poiré A (2019) Deglacial and postglacial paleoseismological archives in mass movement deposits of lakes of south-central Québec. Can J Earth Sci 56:60–76

Trottier AP, Lajeunesse P, Gagnon-Poiré A, Francus P (2020) Morphological signatures of deglaciation and postglacial sedimentary processes in a deep fjord-lake (Grand Lake, Labrador). Earth Surf Process Landf 45:928–947

Tylmann W, Szpakowska K, Ohlendorf C, Woszczyk M, Zolitschka B (2012) Conditions for deposition of annually laminated sediments in small meromictic lakes: a case study of Lake Suminko (northern Poland). J Paleolimnol 47:55–70

van Geel B, Heusser CJ, Renssen H, Schuurmans CJ (2000) Climatic change in Chile at around 2700 BP and global evidence for solar forcing: a hypothesis. Holocene 10:659–664

Wanner H, Solomina O, Grosjean M, Ritz SP, Jetel M (2011) Structure and origin of Holocene cold events. Quat Sci Rev 30:3109–3123

Zolitschka B, Francus P, Ojala AEK, Schimmelmann A (2015) Varves in lake sediments—a review. Quat Sci Rev 117:1–41

Publisher's Note Springer Nature remains neutral with regard to jurisdictional claims in published maps and institutional affiliations.